Infection and Drug Resistance

Dovepress
Taylor & Francis Group

Open Access Full Text Article

ORIGINAL RESEARCH

Diosgenin Promotes Bacterial Clearance in Bladder Epithelial Cells by Regulating Rab27b Expression: A Study Based on Virtual Screening and Experimental Validation

Hao Yin[1,2,*], Jiamin Yin[2,*], Jiahao Zhang[2,*], Xin Wang[2], Enchao Zhou[1]

[1]No. 1 Clinical Medical College, Nanjing University of Chinese Medicine (Jiangsu Province Hospital of Chinese Medicine), Nanjing, 210000, People's Republic of China; [2]Department of Central Laboratory, Suzhou Hospital of Integrated Traditional Chinese and Western Medicine, Suzhou, Jiangsu, 215100, People's Republic of China

*These authors contributed equally to this work

Correspondence: Enchao Zhou; Xin Wang, Email zhouenchao@njucm.edu.cn; frogprince417@sina.com

Introduction: The annual rise in antimicrobial resistance (AMR) rates highlights the critical significance of exploring non-antibiotic therapies for infectious diseases. Urinary tract infection (UTI) is one of the most common bacterial infectious diseases, and uropathogenic Escherichia coli (UPEC), its primary pathogenic bacterium, invades bladder epithelial cells (BECs) to survive and proliferate intracellularly, thereby evading the host's immune clearance. Rab27b mediates the expulsion of intracellular bacteria, and upregulating Rab27b expression can effectively reduce the number of intracellular bacteria.

Methods: In this study, virtual screening and molecular dynamics simulation were used to screen for compounds capable of stably binding to Rab27b. Surface plasmon resonance (SPR) was subsequently performed to validate the direct binding affinity of diosgenin (DSG) to Rab27b. The CCK-8 assay was adopted to determine the experimental concentrations of the compounds for cellular experiments. Western blot (WB), immunofluorescence (IF), colony counting, siRNA transfection and other assays were used to clarify the effects of the screened compounds on Rab27b expression and the number of intracellular bacteria in BECs. Additionally, IF, hematoxylin-eosin (HE) staining, scanning electron microscopy (SEM), and colony counting were employed to investigate the impacts of DSG on Rab27b expression, epithelial integrity, the number of intracellular bacterial CFU, and inflammatory responses in the bladder of mice with UPEC-induced UTI models.

Results: Virtual screening and experimental validation demonstrated that DSG and ST5330591 (ST) could stably bind to Rab27b. DSG upregulated Rab27b protein expression without affecting its mRNA level, suggesting a post-transcriptional mechanism, which contributes to accelerated intracellular bacterial clearance. After Rab27b downregulation via siRNA transfection, DSG lost its ability to clear intracellular bacteria. Furthermore, DSG reduced the number of intracellular Colony-Forming Unit (CFU) in BECs of mice with urinary tract infection, alleviated bladder inflammatory responses, and mitigated the efflux and damage of the bladder epithelial layer.

Conclusion: This study demonstrated that DSG directly binds to Rab27b and upregulates its protein expression via a post-transcriptional mechanism (without altering mRNA levels), thereby promoting the clearance of intracellular UPEC in BECs and exerting therapeutic effects on UTI.

Keywords: virtual screening, diosgenin, urinary tract infection, uropathogenic Escherichia coli, intracellular bacteria

Introduction

Antimicrobial resistance (AMR) has emerged as a major threat to global public health, causing approximately 5 million deaths annually, with its development rate far outpacing the discovery and development of novel antibiotics.[1,2] Therefore, exploring non-antibiotic strategies to ameliorate infectious diseases holds significant clinical and scientific importance.

https://doi.org/10.2147/IDR.S600133
Received: 19 February 2026
Accepted: 18 June 2026
Published: 21 June 2026

Urinary tract infection (UTI) is one of the most prevalent bacterial infectious diseases worldwide, with UPEC as the primary etiologic agent.[3] Uropathogenic Escherichia coli (UPEC) invades BECs in a vesicle encapsulated manner, destroys these vesicles by secreting toxins, and proliferates within the cytoplasm.[4] This not only diminishes the efficacy of antibiotic therapy but also enables UPEC to persist intracellularly, serving as a reservoir for recurrent infections.[5] Previous studies have demonstrated that promoting bacterial clearance within BECs can alleviate bacterial infections.[6] Rab27b is a small GTPase widely expressed in various tissues and organs of mammals, serving as a key molecular switch that exerts central regulatory functions in intracellular vesicular trafficking and fusion events. In the hematopoietic system, Rab27b is highly expressed in platelets, neutrophils and macrophages, where it specifically governs platelet α-granule secretion, neutrophil degranulation and efflux of immune cells, acting as a critical determinant for maintaining normal hemostasis and innate immune responses.[7] In the endocrine system, Rab27b participates in the release of insulin granules from pancreatic β-cells, and its dysfunction directly leads to glucose homeostasis disturbance.[8] In the nervous system, Rab27b mediates the transport and release of synaptic vesicles in neurons, ensuring the precise transmission of neural signals.[9] In the urinary system, Rab27b is abundantly expressed in the superficial umbrella cells of the bladder. It not only plays a pivotal role in maintaining the integrity of the bladder epithelial barrier, but also serves as the core regulatory molecule that mediates the clearance of intracellular UPEC in BECs.[10] Upon UPEC invasion, Rab27b is rapidly activated in BECs and translocates to the membranes of bacteria-containing vesicles, which drives bacterial expulsion and consequently diminishes the intracellular bacterial burden in infected BECs.[11] Thus, Rab27b represents a potential therapeutic target for improving UTI treatment. However, specific therapeutic agents targeting Rab27b remain lacking.

Computer-aided virtual screening, also known as virtual screening, is one of the common methods in early stage drug discovery and drug screening. Essentially, virtual screening involves rapidly identifying potential active compounds from large-scale compound libraries, and is currently a screening approach with a relatively high success rate and cost effectiveness.[12]

Traditional Chinese Medicine (TCM) has accumulated thousands of years of clinical experience in the treatment of UTIs and boasts a vast array of natural products with proven anti-infective and anti-inflammatory activities.[13] The Traditional Chinese Medicine Systems Pharmacology Database and Analysis Platform (TCMSP) is a comprehensive TCM pharmacology research platform that contains 499 Chinese Pharmacopoeia-listed medicinal herbs and their corresponding 29,384 bioactive ingredients, along with comprehensive pharmacokinetic parameters (including oral bioavailability, drug-likeness, and ADME properties) for all compounds.[14] This allows us to pre-screen compounds with favorable drug-like properties before molecular docking, significantly improving the efficiency of virtual screening. Therefore, TCMSP serves as an ideal compound library for screening potential modulators of disease targets from natural products. Therefore, in this study, we selected the TCMSP database as the screening source and integrated virtual screening, molecular dynamics simulations, surface plasmon resonance (SPR), and experimental validation approaches to identify natural small-molecule modulators capable of directly binding to Rab27b. We further validated the regulatory effects of the screened compounds on Rab27b expression at both the transcriptional and protein levels, evaluated their efficacy in clearing intracellular UPEC in BECs, and clarified the functional interaction between the compounds and Rab27b.

Materials and Methods

Virtual Screening

The X-ray crystal structure of Rab27b was retrieved from the Protein Data Bank database. Protein files were processed using AutoDockTools, with polar hydrogen atoms added. A total of 4160 compounds from the Traditional Chinese medicine systems pharmacology database and Analysis Platform natural product library were selected as candidate ligands. Ligand files were converted to PDBQT format using Open Babel. Based on the binding domain of Rab27b, a cubic region of 32.3 Å × 32.3 Å × 32.3 Å was defined (center_x = 17.776, center_y = −5.035, center_z = −19.978). The grid center was determined according to the known binding site of the target to ensure coverage of potential binding sites. The grid resolution was set to 0.05 nm to guarantee high spatial resolution. Grids required for docking were generated using AutoDockTools 1.2.2, and ligand docking was performed within these grids. During docking, ligands underwent multiple rotations and translations within the defined grid region, and Vina optimized the binding energy between ligands

and the protein by simulating different binding modes. Docking calculations included setting the maximum number of rotations and dockings to ensure a comprehensive search for potential binding conformations, outputting multiple possible binding conformations along with their corresponding binding affinities. The conformation of each ligand with the lowest binding affinity was selected for subsequent analysis. Protein-ligand complexes were visualized using PyMOL 2.5. Structural optimization of the docked conformations was performed to further confirm the optimal binding site. Detailed analysis of the binding interface of protein-ligand complexes was conducted using the Protein-Ligand Interaction Profiler and LigPlus.[15]

Molecule Dynamics

Molecular dynamics simulations were performed using AMBER 24 software. Prior to simulations, the AM1-BCC charges of small molecules were calculated via the antechamber module. The small molecules and proteins were described using the GAFF2 small-molecule force field and ff14SB protein force field, respectively. For each system, hydrogen atoms were added using the LEaP module, followed by the solvation of the system in a truncated octahedral TIP3P water box with a 10 Å buffer distance from the solute. Na^+/Cl^- ions were added to neutralize the system charge, and the topology and parameter files required for simulations were finally generated.

Initially, energy minimization was performed on the system. Upon completion of energy minimization, a 200 ps heating stage was carried out under constant volume and controlled heating rate. Subsequently, a 500 ps NVT (isothermal isochoric) ensemble simulation was conducted at 298.15 K to achieve uniform distribution of solvent molecules within the water box. Thereafter, a 500 ps equilibrium simulation was performed for the entire system under isothermal isobaric conditions. Finally, the complex system was subjected to a 100 ns NPT (isothermal isobaric) ensemble simulation with periodic boundary conditions. During the simulations, a cutoff distance of 10 Å was applied for nonbonded interactions, and the Particle Mesh Ewald method was used to calculate long-range electrostatic interactions. The SHAKE algorithm was employed to constrain the bond lengths involving hydrogen atoms, and the Langevin thermostat was used for temperature control with a collision frequency (γ) set to 2 ps^{-1}. The system pressure was maintained at 1 atm, and an integration time step of 2 fs was adopted. Trajectories were saved every 10 ps for subsequent analysis.[16]

Generalized Born Surface Area Binding Free Energy Calculation

The binding free energies between proteins and ligands in all systems were calculated using the Molecular Mechanics/Generalized Born Surface Area method. In this study, the Molecular dynamics trajectories from 90 to 100 ns were employed for the calculations. The specific formula is as follows: $\Delta Gbind = \Delta Gcomplex - (\Delta Greceptor + \Delta Gligand) = \Delta Einternal + \Delta EVDW + \Delta Eelec + \Delta GGB + \Delta GSA$.

Where $\Delta E_{internal}$ represents the internal energy, ΔE_{VDW} denotes the van der Waals interactions, and ΔE_{elec} stands for the electrostatic interactions. ΔG_{GB} and ΔG_{SA} are collectively referred to as the solvation free energy, with ΔG_{GB} being the polar solvation free energy and ΔG_{SA} the nonpolar solvation free energy.[17]

Surface Plasmon Resonance (SPR) Assay Protocol

CM5 sensor chips were mounted on a Biacore T200 system and pre-equilibrated with running buffer until a stable baseline was achieved. All buffers were filtered through 0.22 μm membranes and degassed under vacuum prior to use. Prime, desorb/maintenance wash (performed strictly according to the manufacturer's standard operating procedure, SOP) and system temperature equilibration were completed before any sample injection. Flow cells 1 (FC1) and 2 (FC2) were activated using standard 1-ethyl-3-(3-dimethylaminopropyl) carbodiimide/N-hydroxysuccinimide (EDC/NHS) chemistry. FC1 served as the reference flow cell and was immediately blocked with 1 M ethanolamine (pH 8.5) after activation. For the active flow cell (FC2), recombinant Rab27b protein diluted in 10 mM sodium acetate buffer (pH 5.0) at a concentration range of 20–50 μg/mL was injected until an immobilization level of approximately 8,000–10,000 response units (RU) was reached, followed by blocking with 1 M ethanolamine (pH 8.5) for 7 min. In this study, the final immobilization level of Rab27b was 8,920 RU. Diosgenin working solutions were prepared in running buffer with a final DMSO concentration of 1% and injected in ascending order of concentration. A randomized injection order was alternatively employed to minimize potential system drift artifacts. The flow rate was maintained at 30 μL/min

throughout the assay, with an association phase of 120 s and a dissociation phase of 180 s per injection. The system was thoroughly washed with running buffer between consecutive injections. If non-specific residual binding was detected, a short injection of mild regeneration solution (50 mM NaOH) or extended dissociation time was applied. Given the high sensitivity of small-molecule SPR assays to DMSO-induced refractive index changes, a solvent correction series containing 0.8%, 0.9%, 1.0%, 1.1%, and 1.2% DMSO in running buffer was included in each experimental run. Data processing was performed sequentially using Biacore T200 Evaluation Software (version 3.2): reference flow cell subtraction, blank buffer injection subtraction, baseline normalization, and DMSO solvent correction. The corrected multi-concentration sensorgrams were fitted to a global 1:1 Langmuir binding model to derive the association rate constant (ka), dissociation rate constant (kd), equilibrium dissociation constant (KD), and maximum response (Rmax). Steady-state binding curves were additionally plotted using the average response values at the end of the association phase to cross-validate the KD value obtained from kinetic fitting.[18]

Bacterial Strains and Growth Conditions

The UTI89 strain was obtained from the Central Laboratory of Nanjing University of Chinese Medicine, and the green fluorescent protein (GFP)-tagged UTI89 strain was a kind gift from Yunnan University. Upon receipt of the gifted bacterial stock, we performed shaking culture for passage and cryopreservation. However, for bacterial infection experiments in bladder epithelial cells and mouse UTI models, bacteria were cultured under static conditions using the following specific protocol: Thaw the cryopreserved bacterial stock on ice, streak onto LB agar plates, and incubate at 37°C for 18 h. Pick a single colony and inoculate into 10 mL of LB broth, then incubate statically at 37°C for 18 h. Transfer 10 μL of the above bacterial suspension to 10 mL of fresh LB broth and incubate statically again at 37°C for 18 h.[19] Subsequently, centrifuge the bacterial culture at 1000 × g for 10 minutes and adjust the bacterial concentration to 1×10^8 CFU/mL using sterile phosphate-buffered saline (PBS).

Grouping and Bacterial Infection of Human Transitional BECs

Human 5637 BECs were obtained from iCell Corporation (China, iCell-h232). The cells were cultured in RPMI 1640 medium (Gibco, C11875500BT) supplemented with 10% fetal bovine serum (Gibco, A5256701) under an incubation condition of 37°C and 5% CO_2. All cell experiments were performed using well plates from Corning Inc. (Corning, NY, USA), including 96-well plates for CCK-8 assays, 6-well plates for WB, siRNA transfection and RT-qPCR assays, and 24-well plates for bacterial infection and IF assays. Following seeding into the well plates, the cells were randomly assigned to four groups: the control group, the UPEC group, the DSG group (5uM, AmBeed, A136414), and the ST group (20uM, Sigma, LEYH9B0CB290). After 12 h of pretreatment with the corresponding drugs or vehicle, the medium of all groups except the control group was replaced with UPEC-containing medium at a multiplicity of infection (MOI) of 100.[20]

CCK-8 Assay

Cell viability was assessed by the CCK-8 assay. Logarithmic phase BECs were seeded into 96-well microplates at 1×10^4 cells/well (100 μL/well) with 5 replicates per group. After incubation at 37 °C, 5% CO_2 to the designed time point, 10 μL of CCK-8 reagent was added to each well and incubated for another 1 h under the same conditions. The OD values were measured at 450 nm (reference 630 nm) using a microplate reader.

Bacterial Efflux Assay

After 1 h of infection, the cells were washed and treated with RPMI 1640 medium containing 100 μg/mL gentamicin for 1 h to completely eradicate all extracellular bacteria. At this time, the cells were permeabilized with 0.1% Triton X-100 to determine the initial bacterial CFUs. The remaining cell monolayer was further incubated with 500 μL of fresh medium containing 100 mM methyl-D-mannopyranoside and 25 μg/mL of the bacteriostatic agent trimethoprim (TMP) for 4 h. Following incubation, 100 μL of the pooled culture supernatant was plated onto LB agar plates. The percentage of extracellular bacteria was normalized to the initial intracellular bacterial titer at 2 h.[11]

siRNA Treatment

Human 5637 BECs were seeded in 6-well plates containing RPMI 1640 medium supplemented with 10% FBS, and incubated overnight at 37°C in a 5% CO_2 incubator to reach 70% cell confluence. In a 1.5 mL sterile enzyme-free centrifuge tube, 200 μL of RPMI 1640 medium (serum-free) and 8 μL of GP-transfect-Mate were added and mixed gently. Separately, in another 1.5 mL sterile enzyme-free centrifuge tube, 200 μL of serum-free RPMI 1640 medium and 15 μL of Rab27b-siRNA were mixed thoroughly. The working solution prepared in the first tube was added dropwise to the solution in the second tube, and the mixture was incubated at room temperature for 15 minutes to allow the formation of transfection complexes. The original medium in the 6-well plates was aspirated and replaced with fresh serum-free RPMI 1640 medium. Subsequently, the mixed transfection complex from the previous step was added to each well, and the plates were gently agitated to ensure uniform distribution of the complexes. After incubation at 37°C in a 5% CO_2 incubator for 6 hours, the medium was replaced with complete RPMI 1640 medium supplemented with 10% FBS. At 48 hours post-transfection, total cellular RNA was extracted for RT-qPCR analysis. At 72 hours post-transfection, total cellular proteins were extracted for Western blot analysis to assess the transfection efficiency.

RT-qPCR

Total RNA was isolated from cell samples with the aid of the MolPure Cell/Tissue Total RNA Kit (Yeasen, 19221ES50). Subsequently, the isolated RNA was reverse-transcribed into cDNA utilizing the HS RT SuperMix (YEASEN, 11151ES60). The SYBR qPCR Master Mix (Medicalbio, MR0321) was configured strictly following the manufacturer's protocol. The total volume of each reaction mixture was 20 μL, which contained 0.4 μL of upstream primer, 0.4 μL of downstream primer, 10 μL of SYBR Green Master Mix, 1 μL of cDNA template, and 8.2 μL of nuclease-free water. For data analysis, the 2-ΔΔCt algorithm was employed to calculate relative gene expression levels, with GAPDH serving as the internal reference gene. All primers used in this experiment were custom-synthesized by Sangon Biotech Corporation.The sequences of the primers employed are as follows:

Rab27b-F: TAGACTTTCGGGAAAAACGTGTG.

Rab27b-R: AGAAGCTCTGTTGACTGGTGA.

GAPDH-F: CAGGAGGCATTGCTGATGAT.

GAPDHR: GAAGGCTGGGGCTCATTT.

Animal Grouping and Experimental Protocol

C57BL/6 female mice, 6–8 weeks old, weight (20 ± 3) g, purchased from Jiangsu Qinglongshan Biotechnology, experimental animal license No:SCXK(Su)2021–0001. Mice were routinely fed in the animal experimental center of Suzhou Hospital of Integrated Traditional Chinese and Western Medicine. Mice were housed at 25°C and 50% humidity, alternating light and dark for 12 h/12 h, and were allowed to eat and drink freely. The mice were feded adaptive for 1 week. Mice were randomly divided into four experimental groups: the control group, the UPEC group, the low-dose DSG group (DSGL) and the high-dose DSG group (DSGH). The drug doses in this study were calculated using the body surface area normalization method for human-mouse equivalent dose conversion with reference to published literature, ensuring adequate statistical power while minimizing animal stress and ethical harm.[21] DSG was dissolved in corn oil (vehicle) and administered by oral gavage once daily for 14 consecutive days. The DSG-L group received 48 mg/kg/day, while the DSG-H group received 96 mg/kg/day. Meanwhile, the Control and UPEC groups were gavaged with an equal volume of corn oil alone. Mice were anesthetized by intraperitoneal injection of sodium pentobarbital (30 mg/kg). After confirming the absence of the pain reflex, the mice were fixed on the surgical board, and the urethra and the surrounding skin were disinfected with povidone-iodine. For mice in the UPEC, DSG-L and DSG-H groups, a 100 μL bacterial suspension (1×10^8 CFU/mL) was transurethrally instilled into the bladder to establish a murine UTI model.[22] In contrast, an equal volume of pbs was administered to the control group via the same route as a negative control.

Biochemical Analysis of Blood Samples

Serum levels of alanine aminotransferase (ALT), aspartate aminotransferase (AST), blood urea nitrogen (BUN), and creatinine (Cr) were analyzed using an automatic biochemical analyzer (BS-240VET, Mindray, Shenzhen, China).

Gentamicin Protection Assay

At 6 h post-modeling, mice were placed in a sealed induction chamber and anesthetized with 3% isoflurane delivered in 1 L/min medical oxygen for 5 min. Deep surgical anesthesia was confirmed by complete loss of righting reflex, absence of withdrawal response to toe pinch nociceptive stimulation, and sluggish corneal reflex. Mice were then euthanized by cervical dislocation, and the bladders were harvested aseptically. The bladders were incised along the sagittal plane to fully expose the urothelium, then incubated in PBS containing 100 μg/mL gentamicin for 30 min at room temperature to completely eliminate extracellular adherent bacteria on the bladder surface. After washing 3 times with sterile PBS, each bladder was fully homogenized in 1 mL of sterile PBS. The homogenate was subjected to 10-fold serial dilutions, and 100 μL of the diluted homogenate was plated onto LB agar plates. After inverted incubation at 37 °C for 18 h, the number of intracellular CFUs in BECs was quantified.[23]

Immunofluorescence (IF)

5637 BECs were fixed with 4% paraformaldehyde for 20 min, followed by permeabilization with 0.1% Triton X-100 for 10 min. Subsequently, the cells were blocked with 5% BSA at 37°C for 30 min. After removing the blocking solution with absorbent paper, primary antibodies against Rab27b (Proteintech, 13412-1-AP, 1:500) were added and incubated at 37°C for 1 hour. The cells were then washed and incubated with the Multi-rAb® CoraLite® Plus 594-Goat Anti-Rabbit Recombinant Secondary Antibody (H+L) (Proteintech, RGAR004, 1:500) for 1 hour, followed by treatment with DAPI at 37°C for 10 min. Fluorescence images were captured using a confocal laser scanning microscope, and the fluorescence intensity was analyzed using Image J software.

At 6 hours post-infection, mice were anesthetized with isoflurane and euthanized by cervical dislocation, and the bladders were aseptically harvested. The bladders were fixed in 4% paraformaldehyde, routinely embedded in paraffin, and sectioned into 4 μm-thin slices, which were baked at 65 °C for 1 h in a drying oven. The sections were then deparaffinized in xylene and gradient ethanol, immersed in 1×EDTA antigen retrieval buffer, and subjected to heat-induced antigen retrieval by boiling. After natural cooling, the sections were rinsed three times with sterile PBS. Goat serum was added dropwise onto the sections, which were then blocked at 37 °C for 30 min. Excess goat serum was removed with absorbent paper, followed by incubation with primary antibodies (Uroplakin 3a antibody at 1:100 dilution and Rab27b antibody at 1:500 dilution) at 37 °C for 1 h. The sections were subsequently incubated with secondary antibody (1:500 dilution) at 37 °C for 50 min, and then DAPI staining solution was added for incubation at room temperature for 10 min. After mounting with anti-fade mounting medium, the sections were observed and imaged under a laser scanning confocal microscope (LSCM). The fluorescence intensity of the images from each group was quantified using Image J software.

Hematoxylin-Eosin (HE)

At 6 hours and 72 hours post-infection, mice were anesthetized with isoflurane and euthanized by cervical dislocation, and the bladders were aseptically harvested. Bladders were rinsed with sterile PBS and fixed in 4% paraformaldehyde, then dehydrated through a graded ethanol series, cleared in xylene, embedded in paraffin wax and sectioned into 4 μm-thick sections. Deparaffinized sections were hematoxylin-stained for 2 min (nuclei) and eosin-counterstained for 1 min (cytoplasm). After dehydration, histopathological changes were evaluated under a light microscope.

Scanning Electron Microscopy (SEM)

At 72 hours post-infection, mice were anesthetized with isoflurane and euthanized by cervical dislocation, and the bladders were aseptically harvested. Approximately 1 mm^3 of bladder tissue from each group was fixed in 2.5% glutaraldehyde fixative, post-fixed in osmium tetroxide for 2 h after sterile PBS rinse, and dehydrated through a graded ethanol series. The samples were mounted on copper grids, stained with uranyl acetate, rinsed, and air-dried overnight, then observed and imaged under SEM. The area of exfoliated epithelial cells was quantified by Image J, and the exfoliation ratio of bladder epithelium in each mouse group was calculated as the mean value of three visual fields.

Urine Spot Assay

Mice were housed individually in a quiet environment, and fluorescent-free filter paper was laid flat on the bottom of each cage. The mice were given ad libitum access to food with no water supply provided. After 4 h, the filter paper was removed and air-dried, then illuminated under a fluorescence imager and imaged. The filter paper images were processed using Image J software to quantify the urine spot parameters: the total number of urine spots (the number of spots with an area exceeding 1.7 mm^2 was indicative of micturition frequency); the number of central urine spots (the number of spots in the central 50% area of the filter paper was reflective of abnormal micturition behaviors associated with overactive bladder, OAB).[24]

Enzyme-Linked Immunosorbent Assay (ELISA)

At 72 hours post-infection, mice were anesthetized with isoflurane and euthanized by cervical dislocation, and the bladders were aseptically harvested. The bladders were homogenized in 100 μL ice-cold PBS. The homogenates were centrifuged at 10,000 rpm for 10 minutes at 4 °C, and the supernatants were collected for subsequent ELISA analysis following the manufacturer's instructions. The optical density (OD) was measured at 450 nm with a microplate reader, and the concentration of target analytes in samples was calculated from the standard curve.

Statistical Analysis

Data are presented as mean ± standard error of the mean (SEM). Statistical analyses were performed using GraphPad Prism 8 (GraphPad Software, USA). Normality was assessed by the Shapiro–Wilk test, and homogeneity of variance by the Levene test. For two independent groups, an unpaired two-tailed Student's *t*-test was used when parametric assumptions were met; otherwise, the Mann–Whitney *U*-test was applied. For multiple independent groups, one-way ANOVA followed by Tukey's HSD post hoc test was used for equal variances, Welch's ANOVA followed by Games-Howell for unequal variances, and the Kruskal–Wallis test followed by Dunn's post hoc test for non-parametric data. For multi-timepoint experiments with repeated measurements, two-way repeated measures ANOVA was performed with time as the within-subject factor and treatment as the between-subject factor, followed by Sidak post hoc tests for intergroup comparisons at each time point. For independent multi-timepoint experiments, two-way ANOVA followed by Sidak post hoc tests was used. For CCK-8 assays comparing multiple concentrations to a single control, one-way ANOVA followed by Dunnett's post hoc test was applied. Statistical significance was set at $P < 0.05$.

Results

Results of Virtual Screening

To identify Rab27b modulators, virtual screening via molecular docking was performed on 4160 compounds from the TCMSP database (Figure 1A and B). Five compounds exhibited a binding energy of < −9 kcal/mol (Figure 1C). Specifically, DSG showed a molecular docking binding energy of −10.1 kcal/mol with Rab27b, followed by DSG acetate (−9.9 kcal/mol), schisanlactone A (−9.3 kcal/mol), ST5330591 (ST) (−9.3 kcal/mol), and cabraleone (−9.1 kcal/mol) (Figure 1D–H).

Results of Molecular Dynamics Simulation

Molecular dynamics simulation results demonstrated that Rab27b exhibited superior stability with DSG and ST. Specifically, dynamic behavior analysis of the two complexes revealed that DSG displayed a lower overall root mean square deviation with smaller fluctuations, whereas ST showed a relatively higher root mean square deviation and more significant fluctuations (Figure 2A). Both systems rapidly reached a stable plateau in the initial stage, indicating good overall stability. Notably, the DSG-Rab27b complex maintained a slightly lower root mean square deviation with minimal fluctuations in the plateau phase, while ST-Rab27b exhibited more pronounced fluctuations in the later stage (Figure 2B). The root mean square fluctuation profiles of the two complexes were generally consistent, and the radius of gyration values remained within a stable range for both systems (Figure 2C and D). The DSG-Rab27b complex sustained a higher upper limit of hydrogen bond counts, whereas ST formed a stable but slightly lower average number of

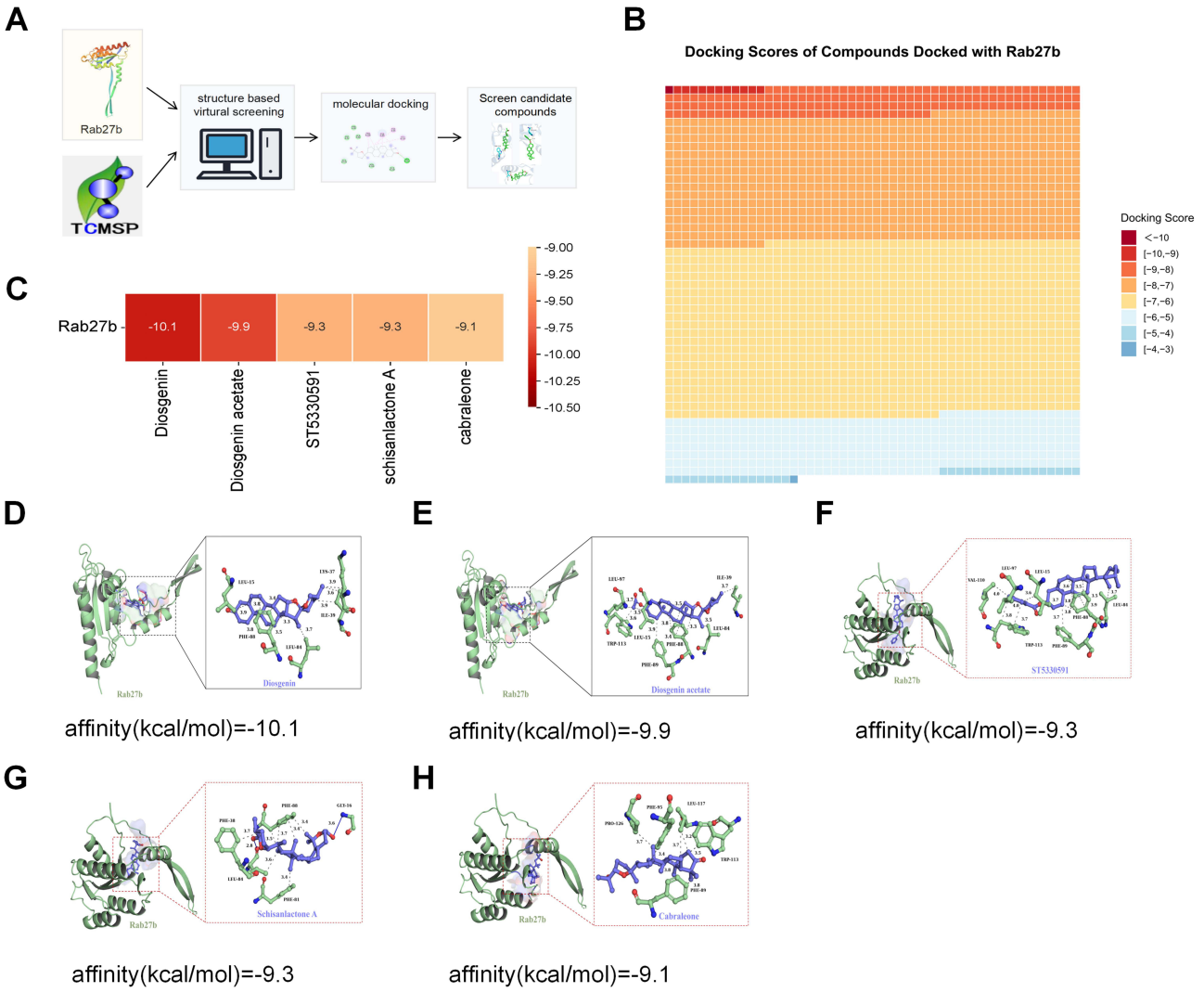

Figure 1 Results of virtual screening. (**A**) The general workflow of virtual screening. (**B**) Binding energies of 4160 compounds with Rab27b. (**C**–**H**) Docking results of compounds with binding energies less than −9.

hydrogen bonds with larger fluctuations (Figure 2E). Additionally, the DSG-Rab27b complex showed a lower overall solvent-accessible surface area, while the ST-Rab27b complex exhibited a slightly higher solvent-accessible surface area with more obvious fluctuations (Figure 2F). Energy decomposition analysis indicated that the binding interface of DSG was stabilized by multiple moderate-strength hydrophobic and polar residues, resulting in a relatively balanced binding energy distribution. In contrast, the binding energy of ST was more concentrated, with significantly enhanced contributions from key hydrophobic and aromatic residues (Figure 2G and H). Free Energy Landscape analysis further confirmed that both complexes exhibited distinct energy basins, indicating stable conformational states (Figure 2I and J).

Effects of DSG and ST on Rab27b Expression Levels in BECs

Among the top five high-affinity compounds, DSG attracted our particular attention due to its well-documented pharmacological activities. It is the major steroidal saponin active constituent of Dioscorea species, the core monarch drug of Wubi Shanyao Pill, a classic TCM formula for rUTIs, and exerts significant anti-inflammatory, immunomodulatory and tissue-protective effects.[25] DSG can inhibit the production of IL-1β, IL-6 and TNF-α,[26] the key mediators of bladder inflammation during urinary tract infections, thus rendering it a highly promising therapeutic candidate for this

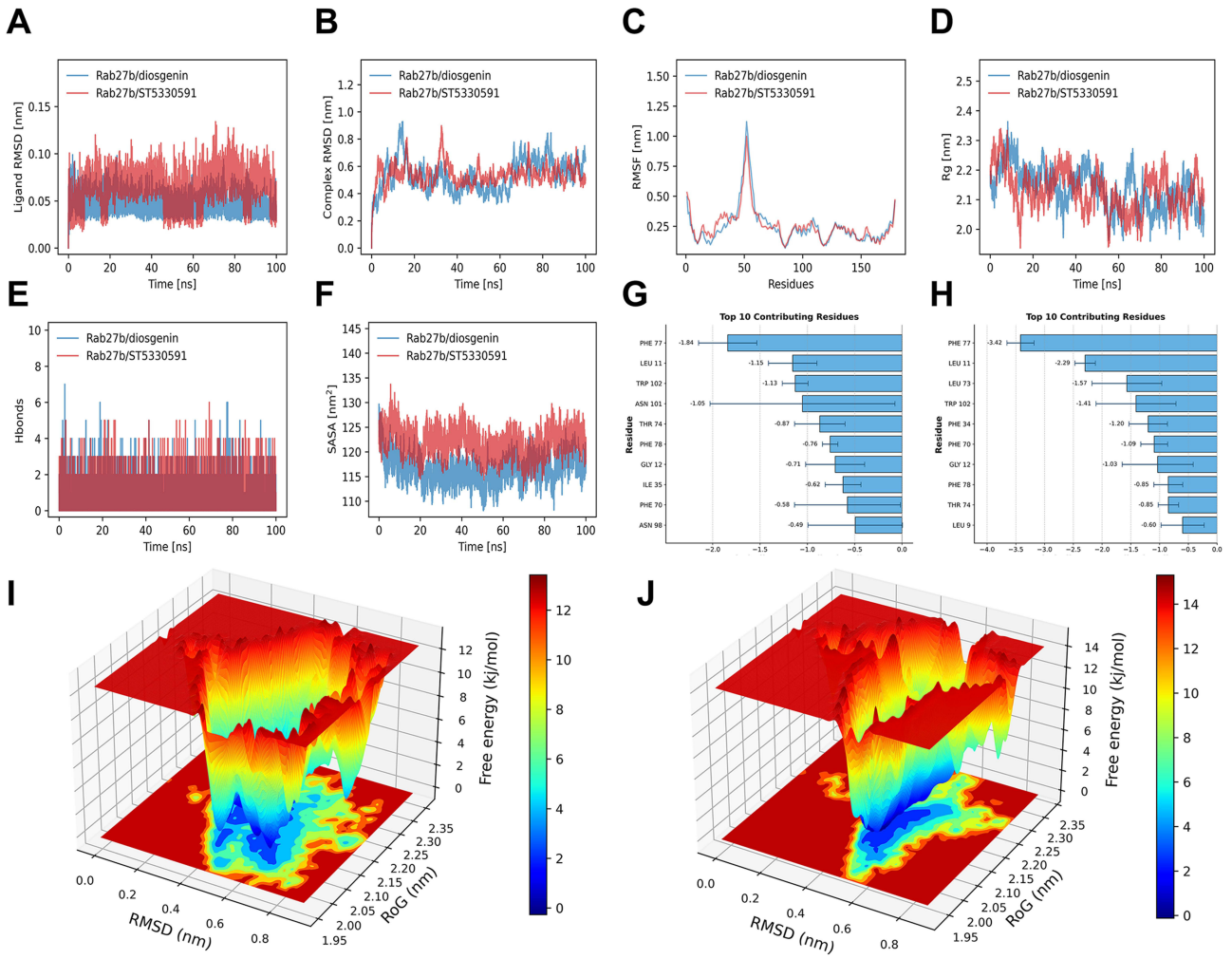

Figure 2 Results of molecular dynamics simulation. (**A**) Ligand RMSD in molecular dynamics. (**B**) Complex RMSD in molecular dynamics. (**C**) Protein RMSF in molecular dynamics. (**D**) Complex Rg in molecular dynamics. (**E**) Number of H-bonds. (**F**) Complex SASA in molecular dynamics. (**G** and **H**) Key amino acid binding energy contributions. (**I** and **J**) Results of free energy landscape.

disease. CCK-8 assay results demonstrated that 5 μM DSG had no significant effect on the viability of BECs ($P > 0.05$), whereas 10 μM DSG significantly impaired cell viability ($P< 0.05$) (Figure 3A). Similarly, 20 μM ST did not affect BECs viability ($P> 0.05$), while 50 μM ST exerted a significant inhibitory effect on cell viability ($P < 0.05$) (Figure 3B). Therefore, 5 μM DSG and 20 μM ST were selected as the optimal concentrations for subsequent experiments. RT-qPCR results showed that neither DSG nor ST affected the mRNA level of *Rab27b* (Figure 3C). WB and IF assays demonstrated that compared with the UPEC group, DSG significantly upregulated the protein expression level of Rab27b in cells ($P < 0.05$), while ST had no significant effect on Rab27b protein expression (Figure 3D–G). To verify the direct binding interaction between DSG and Rab27b, we performed quantitative analysis of their interaction using SPR technology. Rab27b protein was immobilized on the surface of a CM5 sensor chip via amine coupling method, and DSG was flowed over the immobilized protein surface in a concentration gradient of 0.3125–80 μM. After reference flow cell subtraction, blank injection subtraction and DMSO solvent correction, DSG exhibited a clear concentration-dependent binding response on the Rab27b protein surface. Global 1:1 Langmuir kinetic fitting of the multi-concentration sensorgrams yielded an equilibrium dissociation constant (KD) of 8.37 μM, an association rate constant (ka) of 1.47×10^{4} M^{-1} s^{-1}, and a dissociation rate constant (kd) of 1.23×10^{-1} s^{-1} for this interaction (Figure 3H–J).

https://doi.org/10.2147/IDR.S600133

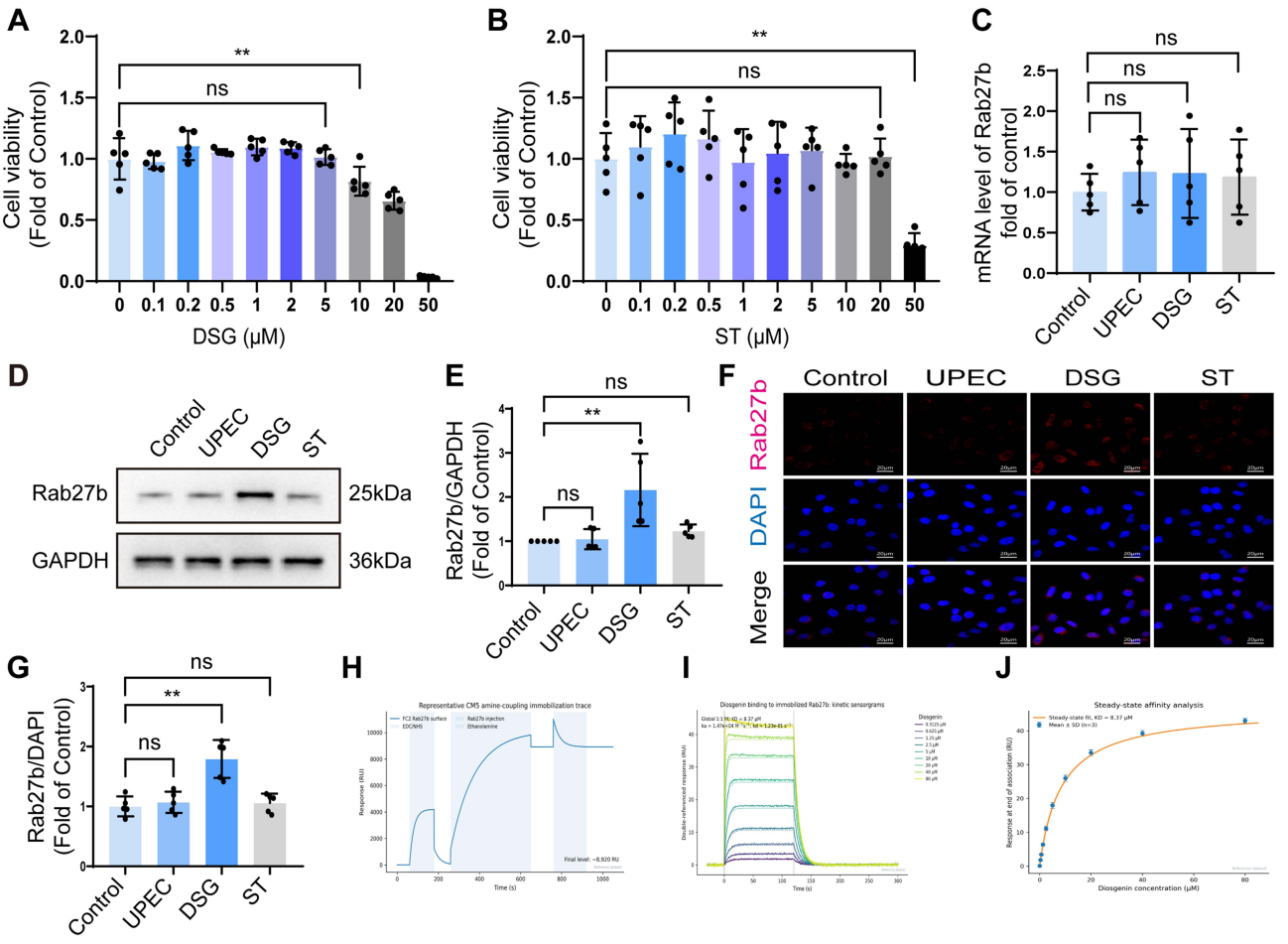

Figure 3 Effects of DSG (5μM) and ST (20μM) on Rab27b expression levels in BECs. (**A** and **B**) The viability of BECs after treatment with varying concentrations of DSG and ST was evaluated using the CCK-8 assay (n=5). (**C**) RT-qPCR analysis of Rab27b mRNA expression levels in different groups (n=5). (**D** and **E**) WB results of the effects of DSG and ST on Rab27b expression levels in BECs (n=5). (**F** and **G**) IF staining results of the effects of DSG and ST on Rab27b expression levels in BECs (n=5). (**H**) Representative amine-coupling immobilization trace of Rab27b protein on a CM5 sensor chip. (**I**) Multi-concentration kinetic sensorgrams of diosgenin binding to Rab27b and global 1:1 Langmuir fitting curves. Solid lines represent experimental data; dashed lines represent model fitting. (**J**) Steady-state affinity analysis based on responses at the end of the association phase. Data points represent the mean ± SD of three independent replicates; the solid curve represents the Langmuir isotherm fitting. Compared with the control group, * means $P < 0.05$, ** means $P < 0.01$.

Effects of DSG on Intracellular Bacterial Load in BECs with Rab27b Downregulation

Rab27b mediates the expulsion of early intracellular bacteria. LB agar plate spreading assays revealed that the number of intracellular bacterial CFU in BECs showed no significant difference across all groups at 2 h post UPEC infection (Figure 4A and B, $P > 0.05$), indicating that DSG and ST do not impair the invasive capacity of UPEC into BECs. At 6 h post UPEC infection, DSG significantly reduced intracellular bacterial load and concomitantly increased bacterial load in the extracellular matrix, suggestive of an elevated rate of intracellular bacterial expulsion (Figure 4A–E, $P < 0.05$), whereas ST had no significant effect on either intracellular or extracellular bacterial load (Figure 4A–E, $P > 0.05$). Agar plate antibacterial activity assays demonstrated that DSG possessed no direct antibacterial activity (Figure 4F), which further confirmed that DSG reduces intracellular bacterial load by promoting intracellular bacterial expulsion rather than by directly inhibiting bacterial proliferation. To validate that DSG exerts its functional effects through the regulation of Rab27b, we knocked down Rab27b expression in BECs using Rab27b-specific small interfering RNA (siRab27b). The efficiency of Rab27b knockdown was verified by qPCR and WB analysis (Figure 4G–I, $P < 0.05$). Subsequent experiments showed that DSG failed to upregulate Rab27b expression in Rab27b-knockdown BECs (Figure 4G–I, $P > 0.05$); concomitantly, it no longer decreased intracellular bacterial load and could not enhance the rate of intracellular bacterial expulsion at 6 h post UPEC infection in these cells (Figure 4J and K, $P > 0.05$).

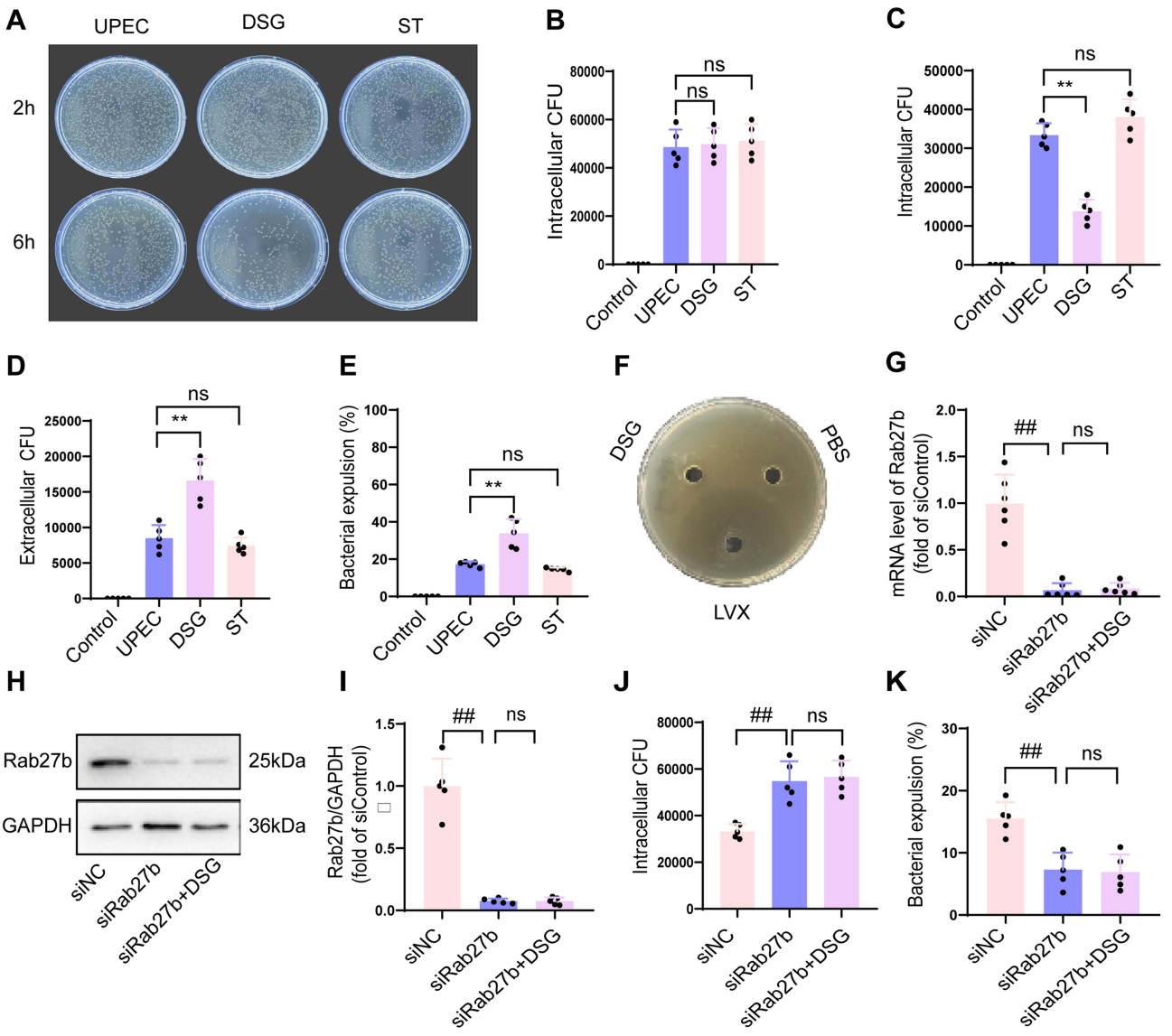

Figure 4 Effects of DSG (5μM) on intracellular bacterial load in BECs. (**A**) Intracellular bacterial colony counts in bladder epithelial cells of each group at 2 h and 6 h post-infection (n=5). (**B**) Intracellular bacterial colony counts in each group at 2 h post-infection (n=5). (**C**) Intracellular bacterial colony counts in each group at 6 h post-infection (n=5). (**D**) Extracellular bacterial colony counts in each group at 6 h post-infection (n=5). (**E**) Intracellular bacterial efflux rates in each group at 6 h post-infection (n=5). (**F**) Results of bacteriostatic assay. (**G**) Rab27b mRNA levels in each group at 48 h post-siRNA transfection (n=5). (**H** and **I**) Rab27b protein levels in each group at 72 h post-siRNA transfection (n=5). (**J**) Intracellular bacterial colony counts in each group at 6 h post-infection (n=5). (**K**) Intracellular bacterial efflux rates in each group at 6 h post-infection (n=5). Compared with the UPEC group, * means $P < 0.05$, ** means $P < 0.01$. Compared with the siNC group, ## means $P < 0.01$.

Effects of DSG on Rab27b Expression and Bacterial Load in the Bladder of UTI Mice

To investigate the safety and therapeutic efficacy of DSG in a mouse model of UPEC infection, we first measured serum liver and kidney function biomarkers. The results showed that neither low nor high dose DSG treatment altered serum levels of ALT, AST, BUN, or Cr compared with the normal control group (Figure 5A–D), indicating a favorable in vivo safety profile of DSG under the experimental conditions used in this study. To investigate the molecular mechanism underlying these effects, we detected Rab27b protein expression levels in bladder tissues by IF staining. The results showed that both low and high dose DSG significantly upregulated Rab27b protein expression in the bladder tissues of UPEC-infected mice compared with the infected model group (Figure 5E and F, $P < 0.05$). An ex vivo bacterial efflux assay further confirmed that bladder epithelial cells from DSG-treated mice exhibited significantly increased bacterial efflux levels at 6 h post-infection ($P < 0.05$, Figure 5G). To further elucidate the effect of DSG on intracellular bacterial clearance, we performed a gentamicin protection assay. The results demonstrated that low and high dose DSG treatment significantly decreased intracellular viable bacterial

https://doi.org/10.2147/IDR.S600133

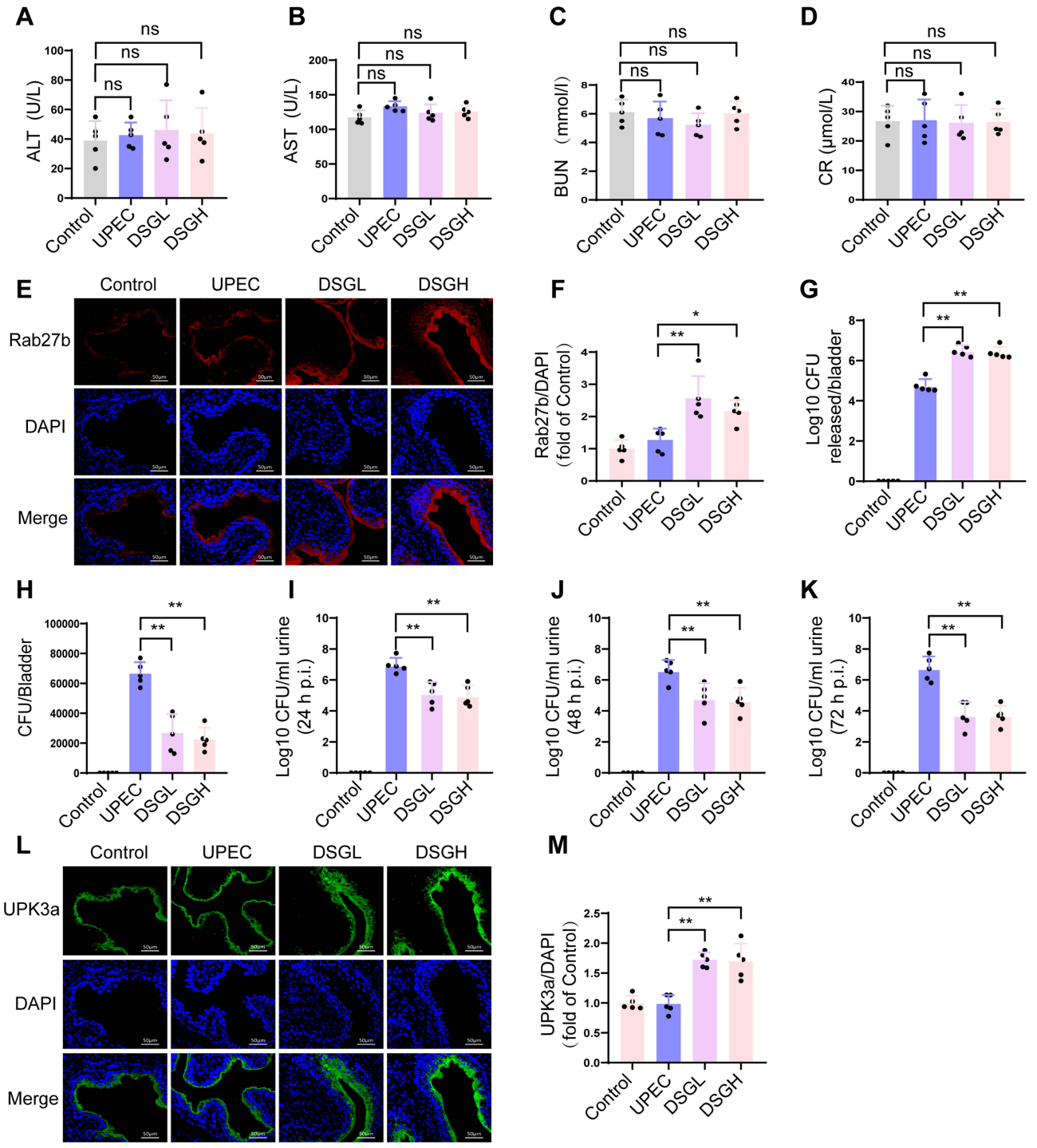

Figure 5 Effects of DSG on Rab27b expression and downstream bacterial clearance in the bladder of UPEC-infected mice. (**A**–**D**) Serum levels of ALT, AST, BUN, and Cr in mice (n=5). (**E**) IF staining of bladder tissues from each group. Rab27b was labeled in red, and cell nuclei were counterstained in blue with DAPI (n=5). (**F**) Quantitative analysis of the fluorescence intensity ratio of Rab27b to DAPI (n=5). (**G**) Ex vivo bacterial expulsion assay showing the number of expelled bacterial CFU from isolated mouse bladder epithelial cells (n=5). (**H**) Gentamicin protection assay showing the number of intracellular bacterial CFU in mouse BECs at 6 h post-infection (n=5). (**I**–**K**) Urinary bacterial load assay showing the number of viable bacterial CFU in mouse urine at 24 h (I), 48 h (J), and 72 h (**K**) post-UPEC infection (n=5). (**L**) IF staining of bladder tissues from each group. UPK3a was labeled in green, and cell nuclei were counterstained in blue with DAPI (n=5). (**M**) Quantitative analysis of the fluorescence intensity ratio of UPK3a to DAPI (n=5). Compared with the UPEC group, * means $P < 0.05$, ** means $P < 0.01$.

counts (CFU) in mouse bladder epithelial cells at 6 h post-infection ($P < 0.05$, Figure 5H). Regarding therapeutic efficacy, urinary bacterial counting revealed that both low and high dose DSG treatment significantly reduced urinary bacterial loads in UPEC-infected mice at 24, 48, and 72 h post-infection ($P < 0.05$, Figure 5I–K). Given that Rab27b exerts a critical regulatory

https://doi.org/10.2147/IDR.S600133

role in the intracellular trafficking of UPK3a protein, we further detected the UPK3a protein expression levels in mouse BECs. Results demonstrated that both low and high doses of DSG significantly upregulated UPK3a protein expression levels in mouse BECs (Figure 5L and M, $P < 0.05$).

Effects of DSG on Bladder Inflammation and Epithelial Integrity in UTI Mice

HE staining was performed on mice bladder tissues at 6 h and 72 h post UPEC infection, and the results demonstrated that extensive inflammatory cell infiltration was observed in the bladder tissues of the UPEC group at 6 h post infection, whereas treatment with low and high doses of DSG markedly reduced inflammatory cell infiltration in bladder tissues (Figure 6A); at 72 h post UPEC infection, extensive exfoliation of BECs was induced by UPEC challenge, while the low and high dose DSG groups significantly alleviated this phenomenon, with a marked reduction in epithelial cell exfoliation

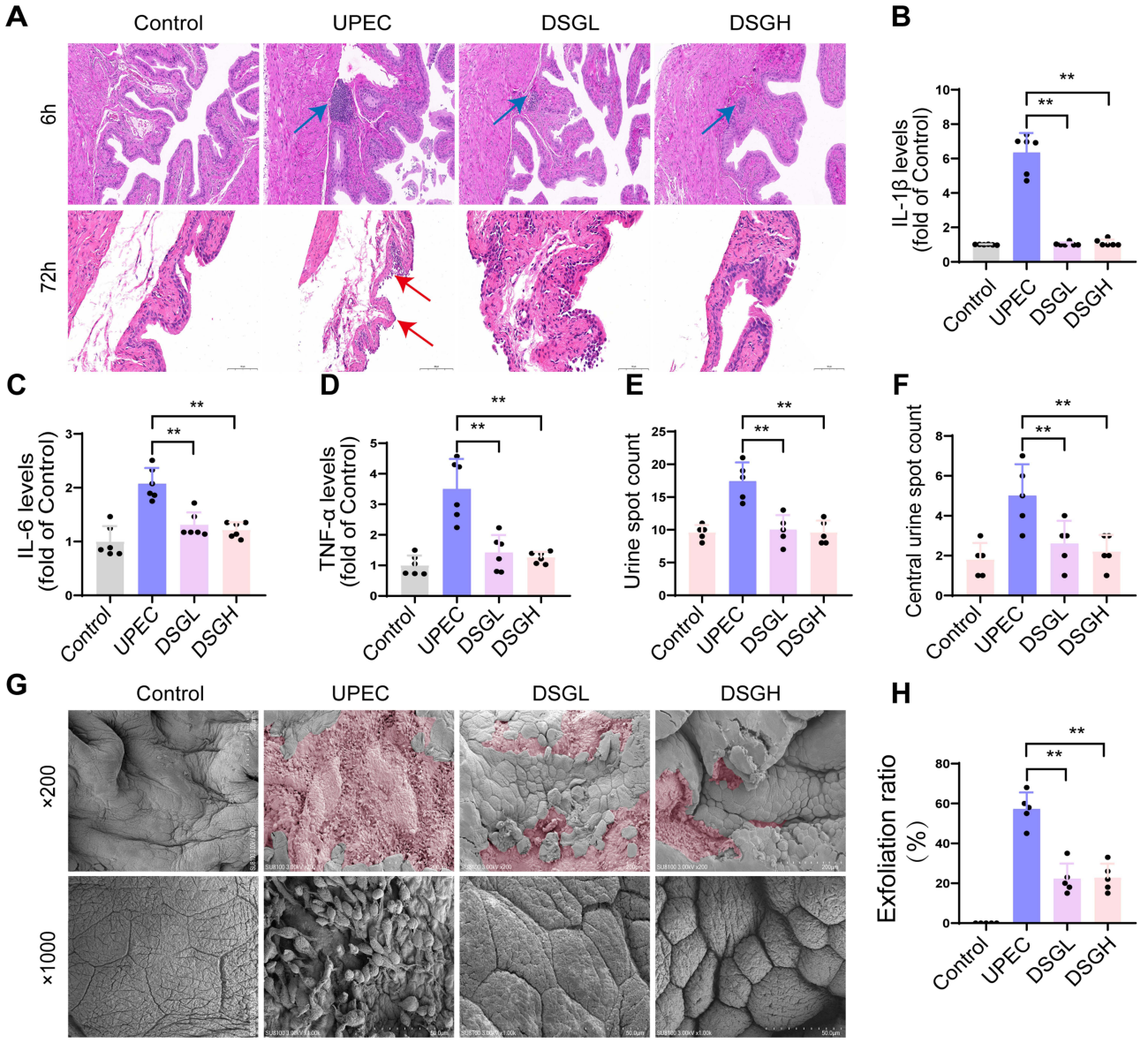

Figure 6 Ameliorative effect of DSG on bladder inflammatory injury in mice with urinary tract infection. (**A**) HE staining of mouse bladders at 6 h and 72 h post-infection; blue arrow: infiltrated inflammatory cells, red arrow: epithelial cell desquamation (n=5). (**B**) IL-1β levels in bladder homogenates detected by ELISA at 72 h post-infection (n=5). (**C**) IL-6 levels in bladder homogenates detected by ELISA at 72 h post-infection (n=5). (**D**) TNF-α levels in bladder homogenates detected by ELISA at 72 h post-infection (n=5). (**E**) Urinary plaque number of mice at 72 h post-infection (n=5). (**F**) Central urinary plaque number of mice at 72 h post-infection (n=5). (**G**) SEM images of mouse bladders at 72 h post-infection; pink: desquamation area of bladder epithelial cells (n=5). (**H**) Desquamation ratio of bladder epithelial cells in each group of mice (n=5). Compared with the UPEC group, * means $P < 0.05$, ** means $P < 0.01$.

https://doi.org/10.2147/IDR.S600133

(Figure 6A). Consistent with previous reports, the levels of proinflammatory cytokines IL-1β, IL-6, and TNF-α were significantly elevated in mice bladder homogenates at 6 h post UPEC infection, whereas treatment with low and high doses of DSG markedly downregulated the levels of these three cytokines (Figure 6B–D, $P < 0.05$). Urinary spot assay results showed that low and high doses of DSG significantly reduced the total urinary spot number and central urinary spot number in UPEC infected mice (Figure 6E and F, $P < 0.05$), indicating that DSG could effectively ameliorate urinary frequency symptoms in UPEC infected mice. SEM analysis of bladder tissues at 72 h post UPEC infection further confirmed that UPEC infection induced extensive exfoliation of BECs, while treatment with low and high doses of DSG markedly reduced BECS exfoliation and preserved epithelial structural stability (Figure 6G and H, $P < 0.05$).

Discussion

AMR has become a global public health crisis. According to the 2022 Lancet series, annual deaths associated with AMR exceed 5 million, of which approximately 1.27 million are directly attributable to resistant infections.[27] The abuse and inappropriate use of antibiotics in urinary tract infections are important selective pressures driving the emergence of UPEC resistant strains.[28] Host-Directed Therapies (HDTs), which enhance host innate bacterial clearance mechanisms, represent a promising alternative strategy, as they act on host cells rather than bacteria, thereby minimizing the risk of bacterial resistance development.[29] In this study, we constructed a library of natural compounds derived from traditional Chinese medicine based on the TCMSP database. Through virtual screening, molecular dynamics simulation, and in vitro and in vivo functional validation, we identified DSG as a candidate compound and demonstrated that Rab27b is an essential molecule for DSG-mediated anti-infection effects.

Rab27b, a member of the Rab small GTPase family, has been extensively studied in tumor biology, immune regulation, and endocrine secretion. Previous studies have shown that Rab27b mediates exosome release in leukemia and breast cancer cells, regulates platelet granule secretion during hemostasis, and participates in insulin granule efflux in pancreatic β cells.[7,9] In the urothelium, Rab27b is a key molecule regulating the trafficking of fusiform vesicles to the apical membrane. Moreover, it has been demonstrated that UPEC specifically localizes to Rab27b-positive vesicles upon invasion, and Rab27b activation promotes the exocytic expulsion of intracellular bacteria.[30] While NRF2 is a key transcriptional regulator of host defense and oxidative stress, our qPCR data demonstrated that DSG dose not alter Rab27b mRNA levels, indicating that Rab27b upregulation occurs through post-transcriptional mechanisms rather than transcriptional activation. Consequently, NRF2-mediated transcriptional regulation is unlikely to account for the observed DSG–Rab27b interaction, and we therefore did not assess NRF2 in the present study. Our findings expand the understanding in this field: Rab27b is not merely a marker of epithelial defense, but its functional upregulation can also be exploited as a therapeutic target. The significant attenuation of DSG anti-infection effects following Rab27b knockdown proves that Rab27b is an essential molecule for DSG-mediated anti-infection effects.

Our data clearly demonstrate that DSG upregulates Rab27b protein expression without altering its transcriptional level, consistent with a post-transcriptional regulatory mechanism. However, the precise molecular link between the direct binding of DSG to Rab27b and the increased protein abundance remains to be elucidated. Potential post-transcriptional regulatory mechanisms include: (1) enhancement of Rab27b protein stability through inhibition of proteasomal or lysosomal degradation pathways;[31,32] (2) increased translation efficiency via regulation of mRNA-binding proteins or microRNAs;[33] (3) promotion of post-translational modifications that extend protein half-life, such as geranylgeranylation, phosphorylation, or deubiquitination;[34] and (4) protein conformational stabilization induced by direct ligand binding.[35] These mechanisms are not mutually exclusive. Future studies are required to systematically distinguish these possibilities and fully elucidate the molecular mechanism underlying this post-transcriptional regulation using approaches including cycloheximide chase assays to determine Rab27b protein half-life, rescue experiments with proteasome and lysosomal inhibitors, quantitative ubiquitination analysis, and polysome profiling.

In addition to the post-transcriptional axis, DSG has been reported to regulate other signaling cascades. Previous studies have found that UPEC invasion of bladder umbrella cells transiently activates the PI3K/Akt signaling pathway in the early stage of infection, promoting bacterial internalization and intracellular survival through the EGFR-PI3K-Akt-mTORC2 axis.[36] In contrast, DSG can induce sustained activation of PI3K/Akt/GSK3β signaling in various disease models, including bone loss and neurological disorders, and this activation is associated with cytoprotective effects.[37]

This suggests that the effects of the PI3K/Akt pathway in urinary tract infections are time-dependent: transient pathogen activation favors invasion, whereas DSG-mediated sustained activation may shift the balance toward host defense. In addition to the PI3K/Akt pathway, DSG has been reported to regulate other signaling cascades, including the STAT2/CMPK2 axis in colitis and GLUR2/GAPDH interactions in epilepsy.[38] These findings suggest that DSG may exert its effects through multiple signaling pathways, but whether these mechanisms regulate Rab27b in bladder epithelium remains to be investigated. Although our study demonstrates that DSG binds directly to Rab27b with moderate affinity (KD = 8.37 μM) and upregulates Rab27b protein levels, we cannot exclude the involvement of other regulatory mechanisms. Future phosphoproteomics and transcriptomics analyses are needed to comprehensively dissect the complete signaling network through which DSG acts on bladder epithelial cells during urinary tract infection.

We found that DSG intervention upregulated UPK3a expression in mouse bladder. UPK3a is a core transmembrane protein of the apical asymmetric unit membrane (AUM) in the urothelium, forming hetero-oligomeric complexes with UPIa to maintain the mechanical barrier and anti-permeability of the bladder epithelium. The relationship between UPK3A expression and UPEC internalization is highly complex. First, UPEC initial adhesion is exclusively mediated by the FimH adhesin, which directly recognizes high-mannose-type N-glycans on the extracellular domain of UPK1A (UPIa);[39] UPK3A dose not participate in the direct binding process of FimH. Therefore, elevated total UPK3A protein levels cannot provide additional adhesion targets for UPEC. Second, UPK3A-mediated internalization signaling depends on its functional activation state rather than mere total protein abundance. Furthermore, the Thr244 residue in the cytoplasmic tail of UPK3A must be specifically phosphorylated by casein kinase 2 (CK2) to initiate downstream calcium signaling and actin cytoskeleton rearrangement.[40]

DSG belongs to the spirostanol-type steroidal sapogenins. Its steroid nucleus shares structural similarities with steroid hormones, but the spirocyclic side chain structure and lack of characteristic steroid hormone side chain groups significantly reduce its hormone receptor affinity.[41] Nevertheless, the potential endocrine disruption risk of long-term high-dose use warrants attention. In this study, mouse DSG doses of 48 mg/kg/day and 96 mg/kg/day were established based on preliminary dose-exploration experiments and confirmed to have no acute toxicity in 14-day pilot experiments. During the 14-day treatment period, no obvious adverse reactions such as behavioral abnormalities, weight loss, or hepatic/renal dysfunction were observed. To mitigate long-term risks, future studies should: (1) comprehensively assess DSG long-term safety in both male and female mice; (2) investigate DSG effects on serum hormone levels and reproductive function; (3) develop bladder-specific local drug delivery formulations (eg., intravesical instillation preparations) to maximize local bladder drug concentration while minimizing systemic exposure. Local delivery is particularly advantageous for urinary tract infection treatment, as it can act directly at the infection site, reducing off-target effect risks.[42]

This study has several limitations. First, although we hypothesize that the PI3K/Akt pathway may mediate DSG regulation of Rab27b protein stability, direct experimental evidence supporting this hypothesis is lacking. Future studies using pharmacological inhibitors and knockout models are needed to validate this signaling axis. Second, although we demonstrate that DSG directly binds to Rab27b and increases its protein level without altering mRNA expression, the exact post-transcriptional mechanism underlying this upregulation—whether via enhanced translation efficiency or inhibition of proteasomal degradation—remains to be elucidated in future studies.Third, this study lacked direct methods to detect Rab27b GTPase activity, which is crucial for understanding its functional activation. Future GTPase activity assays and active Rab27b pull-down experiments will further elucidate DSG mechanisms of action. Fourth, direct evidence demonstrating that DSG promotes exosome- or vesicle-mediated bacterial clearance would significantly strengthen the mechanistic link between Rab27b upregulation and bacterial elimination. However, in acute UPEC infection mouse models, urine contains substantial contaminants, including uromodulin, bacteria, host cell debris, and inflammatory proteins. These contaminants substantially complicate standard exosome isolation methods (eg., ultracentrifugation, precipitation, or size-exclusion chromatography) due to their partial overlap in size and density with exosomes, making it difficult to obtain sufficiently pure exosomal preparations for reliable functional assays.[43,44] We have therefore designated exosome functional validation as a key direction for future research, and plan to first establish an optimized exosome isolation and functional assay system using in vitro cell models to investigate whether DSG promotes UPEC clearance via a Rab27b-dependent vesicular secretion pathway. Fifth, the specific mechanism of DSG

entry into bladder epithelial cells was not directly verified. Based on its lipophilic properties, we speculate that DSG mainly enters cells through passive diffusion; future fluorescent tracer experiments can further confirm this.

Conclusion

This study identifies DSG as a Rab27b modulator through virtual screening and molecular dynamics simulation. DSG upregulates Rab27b expression in BECs, promoting intracellular bacterial expulsion and reducing UPEC load without direct antibacterial effects. In vivo, DSG alleviates bladder inflammation, preserves epithelial integrity, and improves urinary frequency symptoms in UTI mice. These findings establish DSG as a promising host-directed therapeutic candidate for UTI, providing a non-antibiotic strategy to combat bacterial infectious diseases.

Ethical Issue

The experimental procedures of this study comply with all relevant institutional, national, and international guidelines and regulations for animal research and research involving human-related data. All animal housing, handling, anesthesia, and euthanasia operations were carried out in strict accordance with the *Guide for the Care and Use of Laboratory Animals* and the AVMA Guidelines for the Euthanasia of Animals (2020 Edition). The animal study protocol was approved by the Experimental Animal Ethics Committee of Suzhou Hospital of Integrated Traditional Chinese and Western Medicine (Approval No. 2025052).

All publicly available datasets utilized in this study (the Traditional Chinese Medicine Systems Pharmacology Database and Analysis Platform, TCMSP; the Protein Data Bank, PDB) are fully anonymized and de-identified, with no linkable information to specific individuals. This study is therefore exempt from ethical review in full accordance with Items 1 and 2 of Article 32 of the *Measures for Ethical Review of Life Science and Medical Research Involving Human Subjects*, issued by the People's Republic of China on February 18, 2023.

Funding

The project was supported by Basic Research Program of Jiangsu (BK20250515). Natural Science Foundation of Nanjing University of Chinese Medicine (XZR2024061). The Basic Research on Medical and Health Application of Suzhou Science and Technology Program (No. SKY2023105). Suzhou Gusu Health Talent Plan Talent Research Program (No. GSWS2022114). Suzhou Integrated Traditional Chinese and Western Medicine Research Fund (No. SKYD2023243).

Disclosure

Authors declare no conflict of interest.

References

1. Guan C, Torres MDT, Li S, de la Fuente-Nunez C. Computational exploration of global venoms for antimicrobial discovery with Venomics artificial intelligence. *Nat Commun*. 2025;16(1):6446. doi:10.1038/s41467-025-60051-6
2. Liu YY, Wang Y, Walsh TR, et al. Emergence of plasmid-mediated colistin resistance mechanism MCR-1 in animals and human beings in China: a microbiological and molecular biological study. *Lancet Infect Dis*. 2016;16(2):161–168. doi:10.1016/S1473-3099(15)00424-7
3. Timm MR, Russell SK, Hultgren SJ. Urinary tract infections: pathogenesis, host susceptibility and emerging therapeutics. *Nat Rev Microbiol*. 2025;23(2):72–86. doi:10.1038/s41579-024-01092-4
4. Naskar M, Parekh VP, Abraham MA, et al. α-Hemolysin promotes uropathogenic E. coli persistence in bladder epithelial cells via abrogating bacteria-harboring lysosome acidification. *PLoS Pathog*. 2023;19(5):e1011388. doi:10.1371/journal.ppat.1011388
5. Wang C, Bauckman KA, Ross ASB, et al. A non-canonical autophagy-dependent role of the ATG16L1T300A variant in urothelial vesicular trafficking and uropathogenic Escherichia coli persistence. *Autophagy*. 2019;15(3):527–542. doi:10.1080/15548627.2018.1535290
6. Yin H, Zhu J, Jiang Y, et al. Shionone Relieves Urinary Tract Infections by Removing Bacteria from Bladder Epithelial Cells. *Cellular Microbiol*. 2023;2023:3201540. doi:10.1155/2023/3201540
7. Shirakawa R, Higashi T, Tabuchi A, et al. Munc13-4 is a GTP-Rab27-binding protein regulating dense core granule secretion in platelets. *J Biol Chem*. 2004;279(11):10730–10737. doi:10.1074/jbc.M309426200
8. Kasai K, Ohara-Imaizumi M, Takahashi N, et al. Rab27a mediates the tight docking of insulin granules onto the plasma membrane during glucose stimulation. *J Clin Invest*. 2005;115(2):388–396. doi:10.1172/JCI22955
9. Arias-Hervert ER, Xu N, Njus M, et al. Actions of Rab27B-GTPase on mammalian central excitatory synaptic transmission. *Physiol Rep*. 2020;8(9):e14428. doi:10.14814/phy2.14428

10. Miao Y, Bist P, Wu J, et al. Collaboration between Distinct Rab Small GTPase Trafficking Circuits Mediates Bacterial Clearance from the Bladder Epithelium. *Cell Host Microbe*. 2017;22(3):330–342.e4. doi:10.1016/j.chom.2017.08.002
11. Pang Y, Cheng Z, Zhang S, et al. Bladder epithelial cell phosphate transporter inhibition protects mice against uropathogenic Escherichia coli infection. *Cell Rep*. 2022;39(3):110698. doi:10.1016/j.celrep.2022.110698
12. Fara DC, Oprea TI, Prossnitz ER, et al. Integration of virtual and physical screening. *Drug Discov Today Technol*. 2006;3(4):377–385. doi:10.1016/j.ddtec.2006.11.003
13. Flower A, Wang LQ, Lewith G, et al. Chinese herbal medicine for treating recurrent urinary tract infections in women. *Cochrane Database Syst Rev*. 2015;2015(6):CD010446. doi:10.1002/14651858.CD010446
14. Ru J, Li P, Wang J, et al. TCMSP: a database of systems pharmacology for drug discovery from herbal medicines. *J Cheminform*. 2014;6:13. doi:10.1186/1758-2946-6-13
15. Liu S, Wu J, Chen Y, et al. Integrated Virtual Screening Approach Identifies New CYP19A1 Inhibitors. *J Chem Inf Model*. 2025;65(7):3529–3543. doi:10.1021/acs.jcim.5c00204
16. Iftimie R, Minary P, Tuckerman ME. Ab initio molecular dynamics: concepts, recent developments, and future trends. *Proc Natl Acad Sci U S A*. 2005;102(19):6654–6659. doi:10.1073/pnas.0500193102
17. Jiang D, Du H, Zhao H, et al. Assessing the performance of MM/PBSA and MM/GBSA methods. 10. Prediction reliability of binding affinities and binding poses for RNA-ligand complexes. *Phys Chem Chem Phys*. 2024;26(13):10323–10335. doi:10.1039/d3cp04366e
18. Sun B, Xu J, Liu S, Li QX. Characterization of Small Molecule-Protein Interactions Using SPR Method. *Methods Mol Biol*. 2023;2690:149–159. doi:10.1007/978-1-0716-3327-4_15
19. Hung CS, Dodson KW, Hultgren SJ. A murine model of urinary tract infection. *Nat Protoc*. 2009;4(8):1230–1243. doi:10.1038/nprot.2009.116
20. Yin H, Xue Y, Wang X. 1α,25-Dihydroxyvitamin D3 reduces uropathogenic E. coli persistence in bladder epithelial cells by restoring lysosome acidification. *Bangladesh J Pharmacol*. 2025;20:8–15. doi:10.3329/bjp.v20i1.79655
21. Zhang Z, Song C, Fu X, et al. High-dose diosgenin reduces bone loss in ovariectomized rats via attenuation of the RANKL/OPG ratio. *Int J Mol Sci*. 2014;15(9):17130–17147. doi:10.3390/ijms150917130
22. Hannan TJ, Hunstad DA. A Murine Model for Escherichia coli Urinary Tract Infection. *Methods Mol Biol*. 2016;1333:159–175. doi:10.1007/978-1-4939-2854-5_14
23. Beebout CJ, Robertson GL, Reinfeld BI, et al. Uropathogenic Escherichia coli subverts mitochondrial metabolism to enable intracellular bacterial pathogenesis in urinary tract infection. *Nat Microbiol*. 2022;7(9):1348–1360. doi:10.1038/s41564-022-01205-w
24. Hill WG, Zeidel ML, Bjorling DE, Vezina CM. Void spot assay: recommendations on the use of a simple micturition assay for mice. *Am J Physiol Renal Physiol*. 2018;315(5):F1422–F1429. doi:10.1152/ajprenal.00350.2018
25. Sikka S, Shanmugam MK, Siveen KS, et al. Diosgenin attenuates tumor growth and metastasis in transgenic prostate cancer mouse model by negatively regulating both NF-κB/STAT3 signaling cascades. *Eur J Pharmacol*. 2021;906:174274. doi:10.1016/j.ejphar.2021.174274
26. Jung DH, Park HJ, Byun HE, et al. Diosgenin inhibits macrophage-derived inflammatory mediators through downregulation of CK2, JNK, NF-kappaB and AP-1 activation. *Int Immunopharmacol*. 2010;10(9):1047–1054. doi:10.1016/j.intimp.2010.06.004
27. Antimicrobial Resistance Collaborators. Global burden of bacterial antimicrobial resistance in 2019: a systematic analysis, *Lancet*. 2022;399 (10325):629–655. doi:10.1016/S0140-6736(21)02724-0. Epub 2022 Jan 19. Erratum in: Lancet. 2022 Oct 1;400(10358):1102. doi: 10.1016/S0140-6736(21)02653-2
28. Foxman B. Urinary tract infection syndromes: occurrence, recurrence, bacteriology, risk factors, and disease burden. *Infect Dis Clin North Am*. 2014;28(1):1–13. doi:10.1016/j.idc.2013.09.003
29. Kaufmann SHE, Dorhoi A, Hotchkiss RS, Bartenschlager R. Host-directed therapies for bacterial and viral infections. *Nat Rev Drug Discov*. 2018;17(1):35–56. doi:10.1038/nrd.2017.162
30. Joshi CS, Mora A, Felder PA, Mysorekar IU. NRF2 promotes urothelial cell response to bacterial infection by regulating reactive oxygen species and RAB27B expression. *Cell Rep*. 2021;37(3):109856. doi:10.1016/j.celrep.2021
31. Ramakrishna S, Kim YH, Kim H. Stability of zinc finger nuclease protein is enhanced by the proteasome inhibitor MG132. *PLoS One*. 2013;8(1): e54282. doi:10.1371/journal.pone.0054282
32. Dunn Jr WA. Autophagy and related mechanisms of lysosome-mediated protein degradation. *Trends Cell Biol*. 1994;4(4):139–143. doi:10.1016/0962-8924(94)90069-8
33. Ørom UA, Nielsen FC, Lund AH. MicroRNA-10a binds the 5'UTR of ribosomal protein mRNAs and enhances their translation. *Mol Cell*. 2008;30 (4):460–471. doi:10.1016/j.molcel.2008.05.001
34. Wilkinson KD. Ubiquitination and deubiquitination: targeting of proteins for degradation by the proteasome. *Semin Cell Dev Biol*. 2000;11 (3):141–148. doi:10.1006/scdb.2000.0164
35. Celej MS, Montich GG, Fidelio GD. Protein stability induced by ligand binding correlates with changes in protein flexibility. *Protein Sci*. 2003;12 (7):1496–1506. doi:10.1110/ps.0240003
36. Kim WJ, Shea AE, Kim JH, Daaka Y. Uropathogenic Escherichia coli invades bladder epithelial cells by activating kinase networks in host cells. *J Biol Chem*. 2018;293(42):16518–16527. doi:10.1074/jbc.RA118.003499
37. Chen X, Zhang M, Qian L, et al. Diosgenin activates ERα-dependent PI3K/AKT/GSK3β signaling to enhance brain-derived serotonin and alleviate postmenopausal bone loss. *J Adv Res*. 2025;24:S2090. doi:10.1016/j.jare.2025.11.053
38. Qiao X, Zhang L, Wang T, et al. Diosgenin ameliorates colitis by inhibiting mitochondrial DNA synthesis in macrophages via STAT2-CMPK2 pathway. *Phytomedicine*. 2026;150:157605. doi:10.1016/j.phymed.2025.157605
39. Zhou G, Mo WJ, Sebbel P, et al. Uroplakin Ia is the urothelial receptor for uropathogenic Escherichia coli: evidence from in vitro FimH binding. *J Cell Sci*. 2001;114(Pt 22):4095–4103. doi:10.1242/jcs.114.22.4095
40. Thumbikat P, Berry RE, Zhou G, et al. Bacteria-induced uroplakin signaling mediates bladder response to infection. *PLoS Pathog*. 2009;5(5): e1000415. doi:10.1371/journal.ppat.1000415
41. Sethi G, Shanmugam MK, Warrier S, et al. Pro-Apoptotic and Anti-Cancer Properties of Diosgenin: a Comprehensive and Critical Review. *Nutrients*. 2018;10(5):645. doi:10.3390/nu10050645. PMID: 29783752; PMCID: PMC5986524.
42. Nicolle LE. Urinary tract infection: traditional pharmacologic therapies. *Am J Med*. 2002;113(1A):35S–44S. doi:10.1016/s0002-9343(02)01058-6

43. Gonzales PA, Zhou H, Pisitkun T, et al. Isolation and purification of exosomes in urine. *Methods Mol Biol*. 2010;641:89–99. doi:10.1007/978-1-60761-711-2_6
44. Gheinani AH, Vögeli M, Baumgartner U, et al. Improved isolation strategies to increase the yield and purity of human urinary exosomes for biomarker discovery. *Sci Rep*. 2018;8(1):3945. doi:10.1038/s41598-018-22142-x